Improving the local formability of a AA7075 aluminum alloy by laser-induced modification of the alloying concept

Henrik Zieroth[1*], *Marcel* Stephan[2, 3], *Michael* Schmidt[3, 4], and *Marion* Merklein[1]

[1] Institute of Manufacturing Technology (LFT), Friedrich-Alexander-Universität Erlangen-Nürnberg, Egerlandstraße 13, 91058 Erlangen, Germany
[2] Bayerisches Laserzentrum gGmbH (BLZ), Konrad-Zuse-Straße 2-6, 91052 Erlangen, Germany
[3] Friedrich-Alexander-Universität Erlangen-Nürnberg (FAU), Erlangen Graduate School in Advanced Optical Technologies (SAOT), Paul-Gordan-Str. 6, 91052 Erlangen, Germany
[4] Institute of Photonic Technologies (LPT), Friedrich-Alexander-Universität Erlangen-Nürnberg, Konrad-Zuse-Straße 3/5, 91052 Erlangen, Germany

Abstract. With expanding applications in aerospace, automotive, and advanced manufacturing, the need for adaptable materials with tailored mechanical properties is pressing. This study presents a novel approach for selective element adaptation, applied to AA7075 - a high-strength aluminum alloy valued for its exceptional strength but limited by low ductility. Through controlled vaporization of zinc (Zn) and magnesium (Mg), this method enables targeted adjustments in local properties to enhance formability. To evaluate process stability, a comparison was conducted between standard linear vaporization and an advanced double-beam technique, leveraging an optical system that splits and aligns the collimated laser beam for enhanced control. Formability is assessed via 3-point bending tests at varying angles, contrasting vaporized AA7075 with both an exclusively vaporized variant and a silicon-alloyed version approximating the ductility profile of 6xxx alloys. Findings indicate that element-adapted blanks, entitled as Tailored Alloyed Blanks (TAB), achieve significant improvements in localized formability and process stability, establishing a promising technique for the development of adaptable, high-strength materials suited to complex component designs and diverse industrial applications.

Keywords: Tailor Alloyed Blanks (TAB); laser beam welding; element evaporation; aluminum alloys

1 Introduction

Modern engineering designs demand customized materials capable of meeting individual performance targets. [1]. Sectors like aerospace and renewable energy [2] require components that endure high stresses while enabling complex structures. Materials such as aluminum alloys, particularly the high-strength AA7075, have become integral due to their strength-to-weight ratio. However, these alloys are constrained by their limited ductility and susceptibility to cracking, especially during forming and bending operations. This restricts their application in complex structures with intricate geometries or high deformation [3]. Aerospace components, such as fuel-efficient wing spars, require materials that strike a balance between local ductility for a high degree of bending and strength for structural integrity [4]. Traditional methods, such as uniform heat treatments or alloy substitutions, fail to address the dual need for localized ductility in forming-critical areas and strength in load-bearing regions [5]. The need for adaptable materials is further driven by sustainability goals, as lightweight designs reduce material usage and energy costs while meeting environmental standards [4]. Tailored Alloyed Blanks (TAB), laser induced element modified blanks, address these challenges by enabling customization of mechanical properties through selective modification of the alloying concept. TAB enhances ductility in crack-prone regions while maintaining strength in load-bearing areas, overcoming limitations of conventional alloys. The capability to tailor the element concentration for customized material properties addresses the increasing demand for flexibility in manufacturing processes, facilitating the efficient production of customized, application-specific components.

1.1 Laser-based techniques for the local tailoring of aluminum alloys

The production of TAB involves two sequential processes as highlighted yellow in Fig. 1: selective element evaporation and subsequent element alloying. This enables the adjustment of the mechanical properties in forming-critical areas to match the higher ductility of 6xxx series alloys, while the surrounding areas preserve the original strength of the 7xxx series to ensure structural integrity and load-bearing capacity.

* Corresponding author: henrik.zieroth@fau.de

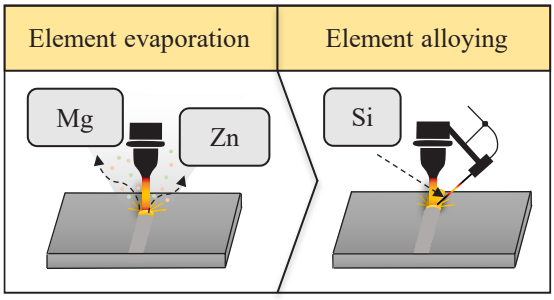

Fig. 1. Process steps for manufacturing TAB

Element adaptation is achieved through keyhole-mode laser processing, as demonstrated schematically in Fig. 2. This process creates a transient, vapor-filled cavity (keyhole) within the material, stabilized by the interplay of vapor pressure, melt pool fluid dynamics, and surface tension forces. These forces collectively balance the keyhole's formation and closure, ensuring control over energy delivery and promote element vaporization [6].

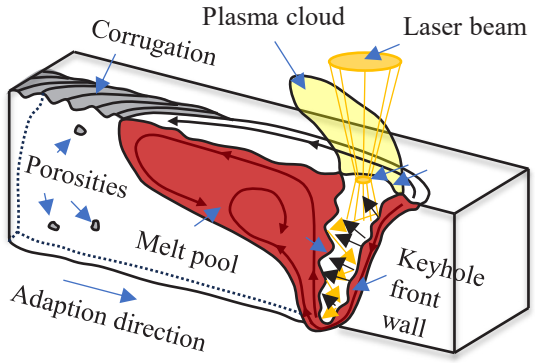

Fig. 2. Laser beam processing in keyhole mode [7]

During this process, magnesium (Mg) and zinc (Zn) are evaporated from the target regions, driven by their lower boiling points (1090 °C for Mg and 907 °C for Zn) compared to aluminum (2470 °C). This vaporization alters the alloy composition, aligning it with the properties of 6xxx series alloys, which are characterized by superior ductility and formability. The local element adaptation in critical zones facilitates the production of complex component geometries with tailored property profiles while reducing the susceptibility to cracking during forming processes. The stability of the keyhole plays a key role in both process efficiency and product quality. Instabilities can result in defects such as spatter, porosity or uneven vaporization, undermining the uniformity of the adapted zones [8]. Within this paper, two distinct laser-based methods for element evaporation are investigated, offering varied approaches to element modification: the single-beam (SB) and dual-beam (DB) techniques, whose procedures are illustrated schematically in Fig. 3. The SB technique utilizes a Gaussian beam profile, characterized by a concentrated energy. This configuration delivers high energy density and precision, making it ideal for the vaporization of Mg and Zn in thin blanks or regions with intricate geometries.

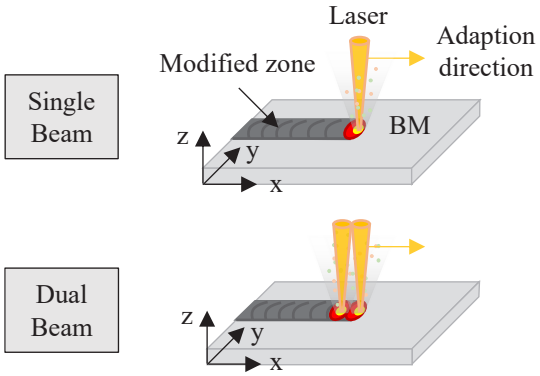

Fig. 3. Laser-based approaches for element evaporation

The smaller keyhole generated by this method reduces the formation of defects such as internal pores and minimizes the heat-affected zone (HAZ). However, the limited power output of single-mode lasers restricts their applicability to thicker materials or zones requiring greater evaporation depth [9]. The DB approach involves splitting the laser into two focal points, resulting in a broader and more uniform energy distribution. While its beam quality is inferior to that of single-mode lasers, this method excels in high-power applications, delivering enhanced performance through its ability to distribute energy more evenly. The larger keyhole generated by this configuration facilitates vaporization of elements in thicker material zones and applications requiring greater depth [10]. Following element evaporation, the areas are further modified in using a wire alloying process, as depicted in Fig. 4, in order to achieve local mechanical properties comparable to those of 6xxx series alloys.

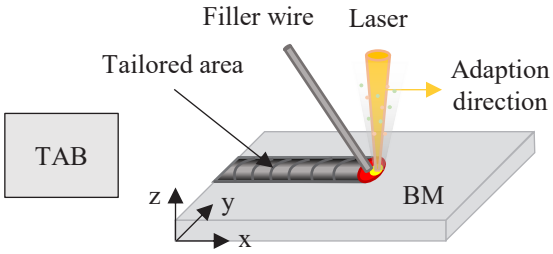

Fig. 4. Schematic overview of the filler wire alloying technique

In this step, an AlSi5 filler wire is introduced into the adapted zones to modify the alloy composition. The incorporation of silicon refines the grain structure and reduces solidification shrinkage, both of which enhance formability in critical bending zones. Additionally, the presence of silicon improves ductility and mitigates hot cracking susceptibility, contributing to the structural stability of the adapted material [11]. The subsequent chapter describes the experimental framework, which includes the characterization techniques used to study the microstructure and elemental composition of the adapted material as well as bending tests to evaluate the formability of TAB.

2 Methods and procedures

The material utilized in this study was provided by Novelis Switzerland SA (Switzerland) in form of sheets with a thickness of 2.0 mm and supplied in the "as- fabricated" (F) condition. In this condition, the material exhibits a low tensile strength of 327.3 MPa ± 0.1 MPa, a uniform elongation of 3.8 % ± 0.1 % and a yield strength of 282.7 MPa ± 2.3 MPa [12]. Table 1 lists the elemental composition of the aluminum alloy as well as the concentration of the target material from which the alloy is to replicate. To remedy the lack of silicon (Si) in the vaporized areas, an AlSi5 wire (MTC GmbH, Meerbusch, Germany) with a thickness of 0.8 mm was added. The boiling points of the main alloying elements - Si, Mg and Zn - were evaluated to determine the extent of element evaporation required to replicate the composition and mechanical properties of a 6xxx aluminum alloy.

Table. 1. Elemental composition and boiling points according to EN-573-3 [12]

Element [wt %]	Si	Mg	Zn
AA7075	0.4	2.1 - 2.9	5.1 - 6.1
AA6061	0.4 - 0.8	0.8 - 1.2	0.25
AlSi5	4.5 - 6.0	0.05	0.10
Boiling point [°C]	3270	1090	907

Evaporation and alloying were conducted using the parameter sets specified in Table 2. A full factorial study was carried out to select the parameter sets, whereby laser power, feed rate, spot size and number of passes were varied in different stages. After evaluating the results of the respective studies with regard to defect development as well as the resulting element concentrations and distributions of Mg, Si and Zn, the specified parameter sets were selected as the most promising compromise.

Table. 2. Parameter sets for the production of TAB

	Laser power [W]	Feed speed [mm/s]	Beam size [µm]	Passes
SB	1500	5	307	2
DB	1500	25	636	1
TAB	1400 + 1600	25	307	2

Two approaches SB and DB optics were investigated for de-alloying whereas only a single-beam optic was used for alloying. All experiments were conducted using a disk laser of type TruDisk 6001 (TRUMPF, Ditzingen, Germany) with a maximum power of 6 kW. The setup consists of a fixed optic of type CSC BEO D70 (TRUMPF, Ditzingen, Germany) and a 3-axis system of type PRO280LM and PRO165 (AEROTECH, Fürth, Germany). The hardness measurements were carried out with a test force of HV 0.1 in accordance to the DIN EN ISO 6507 – 1 [13]. To evaluate the hardness distribution, measurements were mapped across the entire cross-section, encompassing the base material (BM), heat-affected zone (HAZ), and fusion zone (FZ), as shown in Fig. 5.

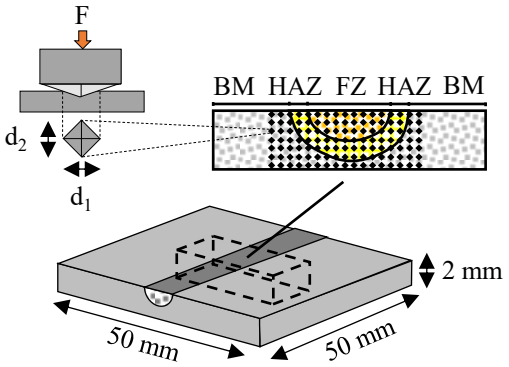

Fig. 5. Vickers hardness measurement

To assess the formability of the evaporated material, a three-point bending test was performed, positioning the adapted zone in the tension-critical region to subject it to maximum bending load. The samples were analyzed using a high-resolution 3D optical measurement system with a stochastic pattern applied to the blank. The system was aligned with the modified area to track bending angle evolution as shown in Fig. 6. The maximum bending angles were analyzed and compared, with the optical images taken prior to failure.

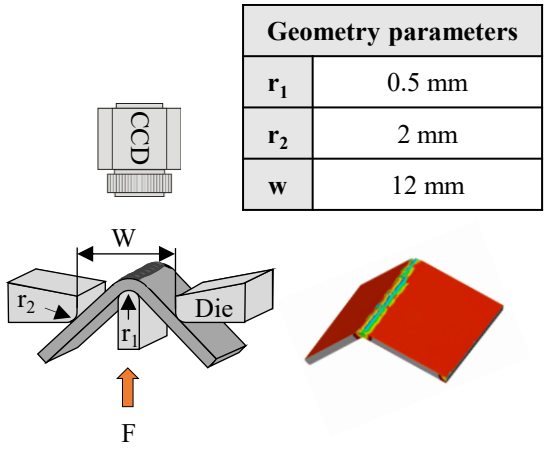

Geometry parameters	
r_1	0.5 mm
r_2	2 mm
w	12 mm

Fig. 6. Illustration of the 3-point bending test setup

Maximum bending angles were measured at three locations: 5 mm after laser entry, at the center of the adapted zone, and 5 mm before laser exit - matching the locations used for the microstructural analysis. The bending angle was determined by fitting regression lines to the legs of the bending curves and calculating their intersections, which were then averaged across the three sections. The microstructural and elemental changes induced by the laser adaptation process were analyzed at the same three predefined locations to evaluate the homogeneity of the element evaporation.

The concentrations of the major alloying elements, Zn and Mg, were quantified using energy dispersion spectroscopy (EDS). For each region, the mean concentrations and standard deviations were calculated to assess compositional variations within the adapted zone. The EDS measurements were performed centered within the customized area. Defects such as pores, cracks, or material loss were analyzed through cross sections obtained from the central adapted zone.

3 Results and discussion

A comparison of the two evaporation strategies reveals variations in the degree of element removal, adaptation depth and defect formation. The SB process, characterized by a low feed rate of 5 mm/s and two traversing passes, achieves the evaporation of over 60 % of the primary alloying elements (Zn and Mg) while maintaining process stability with minimal defect formation, as shown in Fig. 7 The SB process results in an adaptation depth of 1.04 mm ± 0.22 mm, modifying more than half of the 2 mm sheet thickness.

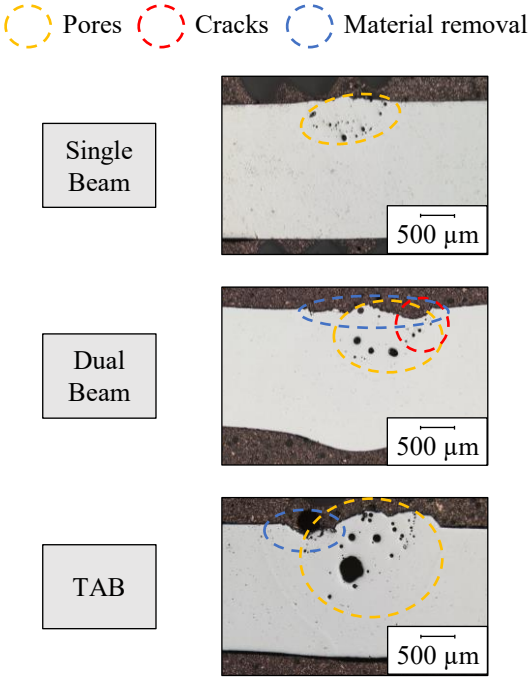

Fig. 7. Cross-sections of varying element adaptations

The low feed rate extends the melting time and facilitates the evaporation of Zn and Mg, while at the same time enabling the dissolution of porosity. This evaporation process minimizes thermal gradients and prevents the formation of cracks. However, the use of two passes intensifies the evaporation by subjecting the material to an additional thermal cycle, which improves element removal but also increases the risk of defect formation. The additional thermal stress destabilizes the dynamics of the keyhole, contributing to the observed porosity, but the overall defect density remains low due to the moderate energy input. By applying the DB process, a higher degree of Zn and Mg evaporation is achieved, reducing the concentrations to 1.0 wt% ± 0.2 wt% and 0.5 wt% ± 0.1 wt% respectively, as shown in Fig. 8. These reductions align the composition further towards the 6xxx series alloys. This enhanced evaporation is attributed to the DB process parameters, including a high feed rate of 25 mm/s, a larger beam diameter from the dual focal configuration, and an extended thermal exposure. The wider keyhole and increased energy input contribute to intensified evaporation, enabling a deeper modification of 1.14 mm ± 0.15 mm, surpassing the penetration achieved with the SB process. However, the benefits of increased evaporation in the DB process come at the expense of structural stability. The intensified energy input destabilizes keyhole dynamics, generating steep thermal gradients and localized stress concentrations. These destabilizing factors lead to the formation of three major defect types: porosity, cracking, and material removal.

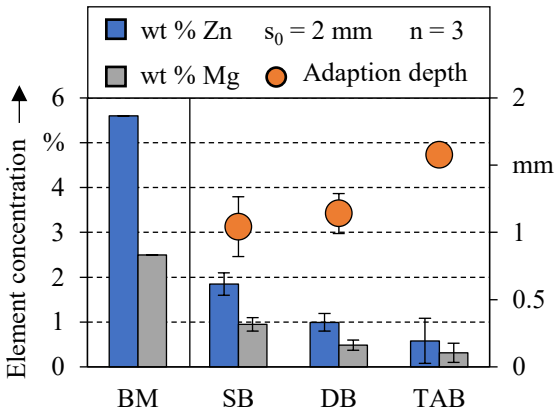

Fig. 8. Comparison of the element concentration in different alloy modifications

The frequent collapse of the wider keyhole during processing generates porosity, while the high evaporation of Zn and Mg alters the material matrix, reducing solid solution strengthening. This weakened material increases susceptibility to cracking, particularly in regions subjected to high thermal stress. Furthermore, the repeated thermal cycling caused by dual laser passes exacerbates localized overheating, which accelerates material removal. The presence of cracks and pores adversely affects the mechanical properties, particularly under tensile load. While the DB process matches the alloy composition of 6xxx series materials and achieves a greater adaption depth of 1.14 mm ± 0.15 mm, the defects created during laser treatment limit its applicability for TAB forming processes. The high occurrence of defects would lead to premature failure under tensile stress. Consequently, the DB process is unsuitable for the production of TAB as the additional laser treatment required for alloying and silicon intermixing would further exacerbate defect formation. For this reason, SB was chosen as the basis for TAB production, which provides a stable material for the subsequent alloying of the filler wire. The TAB, which incorporates AlSi5 wire alloying after SB vaporization, results in a combination of porosity and material removal but no crack formation. The additional thermal cycle introduced during wire alloying causes localized

remelting and re-solidification, leading to gas entrapment and subsequent pore formation. Material removal is attributed to secondary laser interactions with the already vaporized areas, which further increase the mass loss in the pre-weakened structure. The TAB process exhibits the lowest concentrations of Zn and Mg, measured at 0.6 wt% ± 0.5 wt% and 0.3 wt% ± 0.2 wt%. This represents the highest evaporation among the processes evaluated and is a direct consequence of the secondary thermal load during wire alloying. This indicates that the alloy composition of the 6xxx series does not need to be fully achieved during the initial vaporization step, as refinement and element redistribution can still occur during the second process step. By reducing the energy input in the first step, defect volume - such as porosity and cracking - can be minimized, creating a more homogeneous material foundation for subsequent alloying. The adaptation depth achieved with the alloying process significantly increases to 1.58 mm ± 0.08 mm, modifying over three-quarters of the 2 mm sheet thickness. This modification depth can be related to the combined effects of evaporation during the initial SB evaporation and the subsequent wire alloying. The hardness distribution maps for the SB, DB and TAB processes, as depicted in Fig. 9, reveal a consistent softening effect in the modified zones for all three variations.

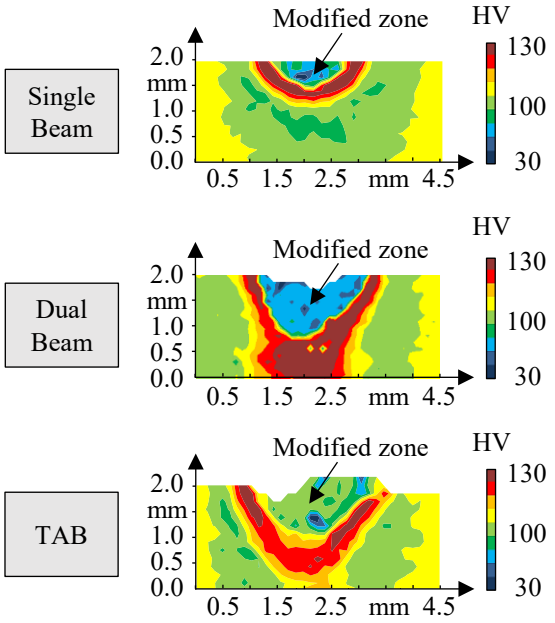

Fig. 9. Microhardness measurements of the element-vaporized (SB, DB) and alloyed samples (TAB)

This reduction in hardness results from the selective evaporation of Zn and Mg weakening the precipitation hardening mechanism of the initial AA7075 alloy. The base material exhibits low hardness due to its as-fabricated (F) condition, where no prior heat treatment has been applied to enhance the mechanical properties. This is consistent with the characteristics of the material listed in the section 2. The focus of this analysis is on the modified region, as it undergoes a compositional transition that alters its precipitation behavior to resemble that of 6xxx-series alloys. Due to the selective evaporation of Zn and Mg and the subsequent addition of Si in the TAB process, the modified region no longer exhibits the precipitation-sensitive characteristics of the original AA7075 composition. As a result, its mechanical properties remain stable over time, showing reduced sensitivity to aging effects. A distinct hardness gradient is observed in the HAZ adjacent to the modified region. The increased hardness in this zone is attributed to the high quenching rates that occur between the base material and the fusion zone, leading to a high potential for precipitation hardening. The rapid cooling restricts grain growth and promotes fine dispersions of strengthening precipitates, resulting in an increase in local hardness [14]. A significant difference between the TAB and the purely vaporized SB and DB zones is the increased hardness modified zone. This increase in hardness is related to the addition of silicon during wire alloying. Silicon refines the microstructure, reduces solidification shrinkage and improves grain refinement, thereby increasing hardness. By contrast, the SB and DB zones, only subjected to element evaporation without subsequent alloying, reveal a more pronounced softening effect due to the lack of reinforcing elements without compensating microstructural changes. The force-displacement curves obtained from the three-point bending tests in Fig. 10 provide a correlation between the mechanical behavior of the adapted areas and the previous analysis. The results indicate the softening effect caused by selective element evaporation, with the DB process exhibiting the lowest bending resistance and premature failure, followed by the SB process, while the TAB achieves the highest ductility and improved bending performance.

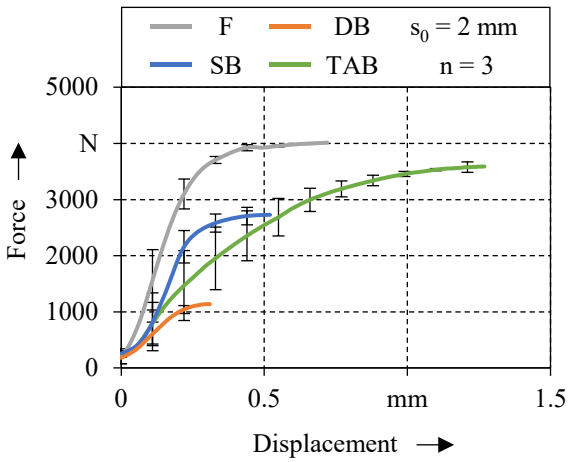

Fig. 10. Load displacement curves of the individual modifications

The DB process, which showed the highest degree of Zn and Mg depletion and the most severe defect accumulation, fails at the lowest displacement of 0.31 mm and under the lowest peak force of 1135 N. This premature failure is attributed to the high porosity and cracking observed in the DB-modified zone. In contrast, the SB process, which exhibited lower element evaporation and fewer defects, withstands a higher force of 2726 N before failure occurs at 0.52 mm displacement. The reduced defect concentration compared to DB allows for greater mechanical stability, delaying failure and increasing the material's load-

bearing capacity. The TAB material demonstrates the most favorable mechanical behavior and achieves a maximum displacement of 1.28 mm - about twice as much as the base material with 0.72 mm - combined with a lower maximum force of 3590 N compared to 4012 N for the base material. The introduction of Si during the wire alloying step refines the grain structure and stabilizes the mechanical response, mitigating excessive softening while preserving enhanced local formability. The bending angle measurements in Fig. 11 confirm the improved formability of the TAB.

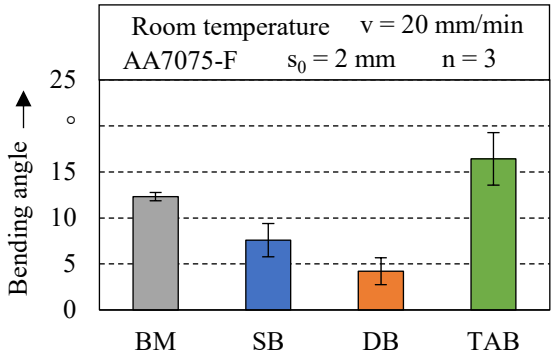

Fig. 11. Bending angle of the individual modifications

TAB achieves the highest bending angle of 16.4 % ± 2.8 % and illustrates that local alloy adaptation increases ductility and extends the forming limits beyond those of AA7075. Despite the reduction in Zn and Mg, the SB and DB specimens do not show any improvement in formability but the opposite, indicating that the composition of a 6xxx series alloy with silicide is required for improved forming behavior under bending load. The standard deviations seen in Figure 11 for both TAB and evaporation conditions are attributed to the presence of porosity and defect formation. The porosity induced during remelting and solidification in the TAB, together with material loss in the SB and DB specimens, contributes to local variations in mechanical properties, resulting in inconsistent deformation behavior.

4 Conclusions

This paper presents a novel laser-based approach for the local element adaptation of materials, demonstrated on AA7075, to enable precise tailoring of mechanical properties and enhance the formability of this alloy. The approach combines selective element evaporation with subsequent silicon alloying, producing Tailored Alloyed Blanks (TAB) with refined microstructure, achieving localized 6xxx-series properties. Bending tests confirmed that pure element evaporation does not enhance formability, as evaporated blanks performed similarly or worse than the base material. In contrast, TAB exhibited the highest bending angles and nearly doubled displacement under lower load, demonstrating the potential of this method to extend forming limits and tailor locally the mechanical properties. Future research will focus on the application of TAB to complex geometries in load-bearing applications.

Acknowledgement

Funded by the German Research Foundation (DFG) - project number 521490180. The authors gratefully acknowledge the support of the Erlangen Graduate School in Advanced Optical Technologies (SAOT) by the Bavarian State Ministry of Science and the Arts.

References

1. R. Rajan, P. Kah, B. Mvola, J. Martikainen, Rev. adv. mater. sci **44,** 383 (2016)
2. S. Ebadi, K. Shahbazi, E. Anbarzadeh, J. environ. friendly mater. **5**, 13 (2021)
3. C. Kammer, Aluminium-Taschenbuch 1.: Grundlagen und Werkstoffe (Beuth, Berlin, 2012)
4. Y. Sun, J. Struct. **57** (2023)
5. M. Merklein, M. Johannes, M. Lechner, A. Kuppert, J. Mater. Process. Technol. **214**, 151 (2014)
6. V. Schultz, P. Woizeschke, J. manuf. mater. process. **2**, 78 (2018)
7. A. Klimpel, J. Mater. Sci. **17** (2024)
8. K. Mundra, T. Debroy, T. Zacharia, S.A. David, Weld. J. (1993)
9. F. Hugger, E. Punzel, M. Schmidt, Lasers Manuf. Mater. Process. (2019)
10. M. Holzer, K. Zapf, S. Kronberger, F. Henkelmann, V. Mann, K. Hofmann, S. Roth, M. Schmidt, Lasers Manuf. Mater. Process. (2017)
11. D. Fabrègue, A. Deschamps, M. Suéry, Mater. Sci. Eng. A **506**, 157 (2009)
12. German Institute for Standardization, Aluminium and aluminium alloys - Chemical composition and form of wrought products - Part 3: Chemical composition and form of products, DIN EN 573 3:2024-03
13. German Institute for Standardization, Metallic materials - Vickers hardness test - Part 1: Test method, DIN EN ISO 6507-1:2024-01
14. L. Zhang, X. Li, Z. Nie, H. Huang, J. Sun, Mater. Des. **83**, 451 (2015)